involve
a journal of mathematics

Linkages of calcium-induced calcium release in a cardiomyocyte simulated by a system of seven coupled partial differential equations

Gerson C. Kroiz, Carlos Barajas,
Matthias K. Gobbert and Bradford E. Peercy

msp

2020 vol. 13, no. 3

INVOLVE 13:3 (2020)
https://doi.org/10.2140/involve.2020.13.399

Linkages of calcium-induced calcium release in a cardiomyocyte simulated by a system of seven coupled partial differential equations

Gerson C. Kroiz, Carlos Barajas,
Matthias K. Gobbert and Bradford E. Peercy

(Communicated by Suzanne Lenhart)

Cardiac arrhythmias affect millions of adults in the U.S. each year. This irregularity in the beating of the heart is often caused by dysregulation of calcium in cardiomyocytes, the cardiac muscle cell. Cardiomyocytes function through the interplay between electrical excitation, calcium signaling, and mechanical contraction, an overall process known as calcium-induced calcium release (CICR). A system of seven coupled nonlinear time-dependent partial differential equations (PDEs), which model physiological variables in a cardiac cell, link the processes of cardiomyocytes. Through parameter studies for each component system at a time, we create a set of values for critical parameters that connect the calcium store in the sarcoplasmic reticulum, the effect of electrical excitation, and mechanical contraction in a physiologically reasonable manner. This paper shows the design process of this set of parameters and then shows the possibility to study the influence of a particular problem parameter using the overall model.

1. Introduction

The leading cause of death in the United States is currently heart disease [Mozaffarian et al. 2015]. In order to continue searching for methods to combat heart disease, it is vital that the heart and its underlying processes are understood with greater depth. The importance of having a greater understanding of the heart provides the motivation for this research.

This project focuses on a single cardiac cell and uses a mathematical model in order to represent the electrical-excitation, calcium-signaling, and mechanical-contraction components of a cardiomyocyte. The study of a single cardiac cell

MSC2010: primary 35K57, 65M08, 65Y05, 68U20, 92C30; secondary 65L04, 65M20, 68W10, 92C37, 92C50.

Keywords: cardiac arrhythmia, calcium-induced calcium release, reaction diffusion equations, finite-volume method, parallel computing.

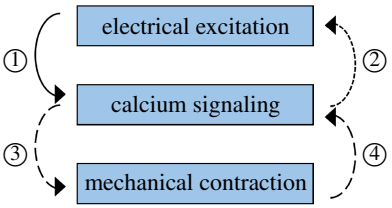

Figure 1. The three components of the model and their links labeled ① to ④.

is important as it is the basic building block of cardiac behavior. The original model for calcium-induced calcium release (CICR) was introduced in [Izu et al. 2001a; 2001b] with a three-variable model and included only calcium signaling. This original model makes up the heart of the calcium-signaling component of the system indicated in Figure 1. Figure 2 sketches the domain of the simulation. We use a hexahedron elongated in the z-direction for the shape of a cell, since the focus of CICR research is on estimating reasonable physiological parameter values. A key of the model in [Izu et al. 2001a; 2001b] is to place the calcium release units (CRUs) on a regular lattice of size, for instance, $15 \times 15 \times 31 = 6{,}975$ throughout the cell; Figure 2 shows three z-planes of 3×3 CRUs as an example. At these many locations, calcium ions are released from the calcium store in the sarcoplasmic reticulum (SR) into the cytosol of the cell, and CRUs can open ("fire") and close repeatedly over time [Izu et al. 2001a; 2001b].

The model was extended for the first time to include the electrical-excitation component in Figure 1 [Alexander et al. 2015], which implemented a one-way interaction from electrical excitation to calcium signaling indicated by link ① in Figure 1. Studies with six variables in [Angeloff et al. 2016] extended the coupling to include a two-way cycle between electrical excitation and calcium signaling by incorporating both links ① and ② in Figure 1. The formulation of the complete eight-variable model for all components in Figure 1 was introduced in [Angeloff et al. 2016], but not all model variables were used in the simulations, and the studies did not incorporate the mechanical system.

The most recent work in [Deetz et al. 2017a; 2017b] studies the introduction of the mechanical-contraction component in Figure 1 by activating the links ③ and ④ in Figure 1. This is facilitated by adding a buffer species whose concentration can be related to the contraction of the cell. Thus, this work uses a model with seven variables to represent the excitation-contraction coupling (ECC) occurring in the cardiomyocyte, in which CICR is the mechanism through which electrical excitation is coupled with mechanical contraction through calcium signaling. The initial results for the newly extended model produce simulations promising in their predictive capability.

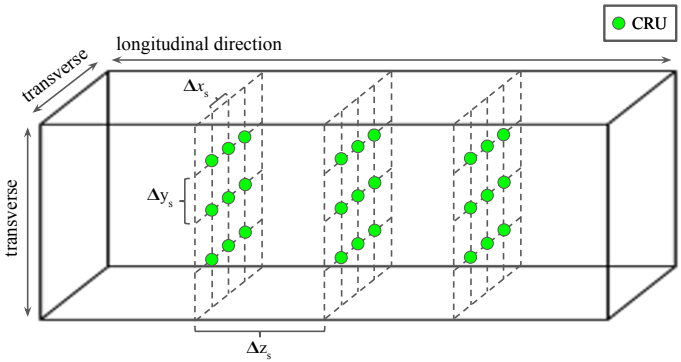

Figure 2. The CRU lattice with spacings Δx_s, Δy_s, Δz_s throughout the three-dimensional cell.

From the previous work, the linkage of the mechanical contraction was existent, but not physiologically correct with the previous set of parameters. The resulting simulations may not have provided realistic behaviors of a cardiac muscle cell. As such, it is important to create a set of parameters with physiologically reasonable simulations. To do this, we reduce the seven-variable model to the three-variable model from [Izu et al. 2001a; 2001b] by setting key parameters to zero. This removes several CICR components: the calcium store in the SR, electrical excitation, and mechanical contraction. By this process, the additional CICR components are negated as they all reduce to zero. From this base case, we reintroduce physiologically reasonable values for these parameters in successive order. First, the corresponding parameter for the calcium store is implemented, reconnecting this component to the system. The selected parameters which negated electrical excitation are then introduced. To complete the system, the key variable connecting mechanical contraction to the rest of the model is included. By creating this set of parameters that includes the CICR components, we are eventually able to study the model as a whole rather than individual components. This paper shows the design process of this set of parameters and then studies the influence of mechanical contraction on the rest of the model for simulations to an extended final time. This shows the possibility of studying the influence of a particular problem parameter using the overall model.

This paper is organized as follows: Section 2 details the seven-variable model used in this work. Section 3 specifies the numerical method used, including its parallelization and implementation. Section 4 is divided into several subsections. Sections 4.1–4.4 show the step-by-step implementation of the CICR components of the seven-variable model. With the complete construction of the set of parameters, Section 4.5 presents a sample application using the new set of parameters. Section 5 collects the conclusions of the work.

2. Dynamics of a cardiac cell

This section details the seven-variable model used in this work. The seven variables of the model are calcium in the cytosol $c(\boldsymbol{x},t)$, a fluorescent dye $b_1^{(c)}(\boldsymbol{x},t)$, a contractile protein (troponin) $b_2^{(c)}(\boldsymbol{x},t)$, a contractile force $b_3^{(c)}(\boldsymbol{x},t)$, calcium in the sarcoplasmic reticulum (SR) $s(\boldsymbol{x},t)$, voltage $V(\boldsymbol{x},t)$, and the potassium gating function $n(\boldsymbol{x},t)$. These are listed in Table 1 with their units and initial values. The evolution of the system is modeled by the system of seven time-dependent, coupled, nonlinear reaction diffusion equations

$$\begin{aligned}\frac{\partial c}{\partial t} &= \nabla\cdot(D_c\nabla c) + R_{b_1}^{(c)} + R_{b_2}^{(c)} \\ &\quad + (J_{\mathrm{CRU}} + J_{\mathrm{leak}} - J_{\mathrm{pump}}) + \kappa J_{\mathrm{LCC}} + (J_{m_{\mathrm{leak}}} - J_{m_{\mathrm{pump}}}), \quad (1)\end{aligned}$$

$$\frac{\partial b_1^{(c)}}{\partial t} = \nabla\cdot(D_{b_1^{(c)}}\nabla b_1^{(c)}) + R_{b_1}^{(c)}, \quad (2)$$

$$\frac{\partial b_2^{(c)}}{\partial t} = \nabla\cdot(D_{b_2^{(c)}}\nabla b_2^{(c)}) + R_{b_2}^{(c)}, \quad (3)$$

$$\frac{\partial b_3^{(c)}}{\partial t} = \nabla\cdot(D_{b_3^{(c)}}\nabla b_3^{(c)}) + R_{b_3}^{(c)}, \quad (4)$$

$$\frac{\partial s}{\partial t} = \nabla\cdot(D_s\nabla s) - \gamma(J_{\mathrm{CRU}} + J_{\mathrm{leak}} - J_{\mathrm{pump}}), \quad (5)$$

$$\begin{aligned}\frac{\partial V}{\partial t} &= \nabla\cdot(D_v\nabla V) + \tau_v\frac{1}{C}\Bigg[I_{\mathrm{app}} - g_L(V-V_L) - g_K n(V-V_K) \\ &\quad - \frac{2F}{S\tau_{\mathrm{flux}}}J_{\mathrm{LCC}} - \omega(J_{m_{\mathrm{leak}}} - J_{m_{\mathrm{pump}}})\Bigg], \quad (6)\end{aligned}$$

$$\frac{\partial n}{\partial t} = \nabla\cdot(D_n\nabla n) + \tau_v\lambda_n\cosh\left(\frac{V-V_3}{2V_4}\right)(n_\infty(V) - n). \quad (7)$$

The domain in our model is a hexahedron

$$\Omega = (-6.4, 6.4)\times(-6.4, 6.4)\times(-32.0, 32.0) \quad (8)$$

with units μm with isotropic CRU distribution as sketched in Figure 2 with a sample of three z-planes of 3×3 CRUs. A typical cell has on the order of $15\times15\times31 = 6{,}975$ calcium release units (CRUs) throughout the cell. A cell is reasonably modeled by the hexahedral shape elongated in the z-direction, since the focus of CICR research is on estimating correct physiological parameter values. The model uses no-flux boundary conditions for all dependent variables, so that no species escapes or enters the cell through the domain boundary $\partial\Omega$; this corresponds to the goal of modeling the behavior of a single cell. To finish the well-posed statement of an initial-boundary value problem of parabolic type, such as the seven

variable	definition	initial value	
$\boldsymbol{x}$	spatial position variable (x, y, z)	μm	
t	time variable	ms	
$c(\boldsymbol{x}, t)$	calcium in the cytosol	$c_0 = 0.1\,\mu$M	A
$b_1^{(c)}(\boldsymbol{x}, t)$	free fluorescent dye in the cytosol	$45.918\,\mu$M	A
$b_2^{(c)}(\boldsymbol{x}, t)$	free troponin in the cytosol	$111.818\,\mu$M	A
$b_3^{(c)}(\boldsymbol{x}, t)$	inactive actin-myosin cross-bridges	$145.20\,\mu$M	C
$s(\boldsymbol{x}, t)$	calcium in the SR	$s_0 = 10{,}000\,\mu$M	A
$V(\boldsymbol{x}, t)$	membrane potential (voltage)	-50 mV	B
$n(\boldsymbol{x}, t)$	fraction of open potassium channels	0.1	B

Table 1. Independent and dependent variables of the seven-variable model and their initial conditions. The concentration unit M is shorthand for mol/L (moles per liter). The last column indicates which system component in Figure 1 contains each dependent variable: A = calcium signaling, B = electrical excitation, C = mechanical contraction.

equations (1)–(7), values for all dependent variables need to be specified at the initial time $t = 0$, which is done by the values in Table 1.

The following text will detail the mathematical model for each of the three system components in Figure 1 containing the variables in Table 1: The calcium-signaling component contains variables c, $b_1^{(c)}$, $b_2^{(c)}$, and s. The electrical-excitation component contains V and n and is connected to the calcium signaling in both the feedforward and feedback directions, represented by links ① and ②. The mechanical-contraction component contains $b_3^{(c)}$ and is also connected to the calcium signaling in both the feedback and feedforward directions represented by links ③ and ④.

The initial value $c_0 = 0.1\,\mu$M is the basal level of calcium in the cytosol, which is a physiologically measured value for the system at rest. The initial values for all buffer species $b_1^{(c)}$, $b_2^{(c)}$, and $b_3^{(c)}$ are calculated from their reaction rates such that no reactions take place for cytosol calcium $c = c_0$ at rest. The initial value $s_0 = 10{,}000\,\mu$M for calcium in the SR is selected very high, so that the amount of calcium in the store is not a limiting factor for the release of calcium at first; this is a common technique to promote nontrivial behavior of the model in simulations. The initial values for membrane potential V and the fraction of open potassium channels n represent the resting state of the electrical system of the cell.

Tables 2 and 3 contain the parameters in the PDEs of the calcium system with their values (if fixed) and units; some of the values are varied in the experiments in Section 4. The coefficients D_c, $D_{b_i^{(c)}}$, and D_s are the 3×3 diffusivity matrices for

Ca^{2+} in the cytosol, buffer species i in the cytosol, and Ca^{2+} in the SR, respectively; these matrices are diagonal, as indicated in Table 2, with potentially different values in the x-, y-, z-directions, or potentially zero, if the species does not diffuse.

variable	definition	values/units
D_c	diffusivity matrix for $c(\boldsymbol{x}, t)$	diag(0.15,0.15,0.3) μm^2/ms
$D_{b_1^{(c)}}$	diffusivity matrix for $b_1^{(c)}$	diag(0.01,0.01,0.02) μm^2/ms
$D_{b_2^{(c)}}$	diffusivity matrix for $b_2^{(c)}$	diag(0.00,0.00,0.00) μm^2/ms
$D_{b_3^{(c)}}$	diffusivity matrix for $b_3^{(c)}$	diag(0.00,0.00,0.00) μm^2/ms
D_s	diffusivity matrix for $s(\boldsymbol{x}, t)$	diag(0.78,0.78,0.78) μm^2/ms
$R_{b_i}^{(c)}$	reactions of cytosol Ca^{2+} with buffers	μM/ms
$k_{b_1^{(c)}}^+$	forward reaction coefficient for $b_1^{(c)}$	0.080 $(\mu\text{M ms})^{-1}$
$k_{b_2^{(c)}}^+$	forward reaction coefficient for $b_2^{(c)}$	0.100 $(\mu\text{M ms})^{-1}$
$k_{b_3^{(c)}}^+$	forward reaction coefficient for $b_3^{(c)}$	0.040 ms^{-1}
$k_{b_1^{(c)}}^-$	reverse reaction coefficient for $b_1^{(c)}$	0.090 ms^{-1}
$k_{b_2^{(c)}}^-$	reverse reaction coefficient for $b_2^{(c)}$	0.100 ms^{-1}
$k_{b_3^{(c)}}^-$	reverse reaction coefficient for $b_3^{(c)}$	0.010 ms^{-1}
γ	ratio of volume of cytosol to SR	14
$b_{1,\text{total}}^{(c)}$	total amount of $b_1^{(c)}$ in the cytosol	50 μM
$b_{2,\text{total}}^{(c)}$	total amount of $b_2^{(c)}$ in the cytosol	123 μM
$b_{3,\text{total}}^{(c)}$	total amount of $b_3^{(c)}$ in the cytosol	150 μM
J_{leak}	calcium leak from SR	0.3209684 μM/ms
J_{pump}	calcium transfer from cytosol to SR	μM/ms
V_{pump}	maximum pump rate	4 μM/ms
K_{pump}	pump sensitivity to Ca^{2+}	0.184 μM
n_{pump}	Hill coefficient for pump function	4.0
J_{CRU}	calcium flux from SR to cytosol via CRUs	μM/ms
$\mathcal{O}$	gating function for J_{CRU}	0 or 1
J_{prob}	probability of CRU opening	0 to 1
$\boldsymbol{x}_s$	three-dimensional vector for CRU location	μm
Δx_s	CRU spacings in x	0.8 μm
Δy_s	CRU spacings in y	0.8 μm
Δz_s	CRU spacings in z	2.0 μm
$\hat{\sigma}$	maximum rate of release	110 μM μm^3/ms
$\delta(\boldsymbol{x}-\hat{\boldsymbol{x}})$	Dirac delta distribution	$1/\mu$m^3
u_{rand}	uniformly distributed random variable	0 to 1
P_{max}	maximum probability for release	0.3
K_{prob_c}	sensitivity of CRU to cytosol calcium	2 μM
n_{prob_c}	Hill coefficient for probability function	4
K_{prob_s}	sensitivity of CRU to SR calcium	550 μM
n_{prob_s}	Hill coefficient for probability function	4

Table 2. Parameters for calcium signaling.

variable	definition	values/units
D_v	diffusivity matrix for $V(\boldsymbol{x}, t)$	diag(100,100,100) μm^2/ms
D_n	diffusivity matrix for $n(\boldsymbol{x}, t)$	diag(0,0,0) μm^2/ms
τ_v	scaling factor in voltage equation	0.1 μM μm^3/ms
τ_{flux}	scaling factor in J_{LCC} term	0.1
V_1	potential at which $m_\infty = 0.5$	-1.0 mV
V_2	reciprocal of slope of voltage dependence of m_∞	15.0 mV
V_3	potential at which $n_\infty = 0.5$	10.0 mV
V_4	reciprocal of slope of voltage dependence of n_∞	14.5 mV
V_L	equilibrium potential for leak conductance	-50 mV
V_{Ca}	equilibrium potential for Ca^{2+} conductance	100 mV
V_K	equilibrium potential for K^+ conductance	-70 mV
C	membrane capacitance	20 μF/cm^2
I_{app}	applied current	50 μA/cm^2
g_L	max./instantaneous conductance for leak	2 mmho/cm^2
g_{Ca}	max./instantaneous conductance for Ca^{2+}	4 mmho/cm^2
g_K	max./instantaneous conductance for K^+	8 mmho/cm^2
m_∞	fraction of open calcium channels at steady state	0 to 1
n_∞	fraction of open potassium channels at steady state	1
λ_n	max. rate constant for opening of K^+ channels	0.1 ms^{-1}
J_{LCC}	influx of calcium via L-type calcium channels	μM/ms
S	surface area of the cell	3604.48 μm^2
F	Faraday constant	95484.56 C/mol
κ	scaling factor of J_{LCC}	0.1
ω	feedback strength (scaling factor) for Ca^{2+} efflux	100 μA ms/μM cm^2
$J_{m_{\text{leak}}}$	leak of calcium via L-type calcium channels	0.1739493 μM/ms
$J_{m_{\text{pump}}}$	pump of calcium via L-type calcium channels	μM/ms
$V_{m_{\text{pump}}}$	max. pump rate	0.3 μM/ms
$n_{m_{\text{pump}}}$	membrane pump Hill coefficient	4
$K_{m_{\text{pump}}}$	membrane pump Ca^{2+} sensitivity	0.18
$[XB]_0$	initial concentration of active cross-bridges	142.6805 μM
ε	shortening factor	0 to 1
F_{max}	max. force by actin-myosin cross-bridges	1 μN
k_s	stiffness of actin filament	0.025 N/m

Table 3. Parameters for electrical excitation and mechanical contraction with base units of mho $= (s^3A^2)/(kg\,m^2)$ and F $= (s^4A^2)/(kg\,m^2)$.

The calcium signaling portion of the model consists of the equations (1)–(5). The reaction terms $R_{b_i}^{(c)}$ describe the reactions between calcium and the buffer species. They are the connections between (1)–(4). More precisely, we have

$$R_{b_1}^{(c)}(c, b_1^{(c)}) = -k_{b_1^{(c)}}^{+} c b_1^{(c)} + k_{b_1^{(c)}}^{-}(b_{1,\text{total}}^{(c)} - b_1^{(c)}), \tag{9}$$

for reaction between cytosol calcium and the fluorescent dye.

When troponin binds to Ca^{2+}, the protein as a whole changes shape: this not only allow actin-myosin cross-bridges to form, but also traps the calcium in its connection to the troponin so that the disassociation rate of troponin binding to Ca^{2+} decreases dramatically. To account for this, the shortening factor ε describes how the separation of troponin and calcium has been physically, but not chemically, impaired. When there are open CRUs that, as a result, release calcium in the cytosol, this chain of changes of variables increases in severity. However, after $t = 5$ ms of being open, the CRUs close and remain in a refractory state for $t = 100$ ms. During this period, the unbinding of troponin and calcium increase to the initial rate of unbinding and myosin cross-bridges become inactive. This results in these terms returning to their original states. This cycle is continuous triggered and reset by the calcium waves produced by a cardiomyocyte. Note, again, that $R_{b_2}^{(c)}$ remains a function of cytosol calcium concentration $c(\boldsymbol{x}, t)$ by its equation

$$R_{b_2}^{(c)}(c, b_2^{(c)}) = -k_{b_2^{(c)}}^{+} c b_2^{(c)} + \left(\frac{k_{b_2^{(c)}}^{-}}{\varepsilon}\right)(b_{2,\text{total}}^{(c)} - b_2^{(c)}), \tag{10}$$

with

$$\varepsilon = \exp\left(F_{\max} k_s \left(\frac{b_{3,\text{total}}^{(c)} - b_3^{(c)} - [XB]_0}{b_{3,\text{total}}^{(c)} - [XB]_0}\right)\right) \tag{11}$$

and $[XB]_0 = b_{3,\text{total}}^{(c)} - b_3^{(c)}(\boldsymbol{x}, 0)$. This shortening factor ε links ③ and ④ in Figure 1. It is important to note that the disassociation rate of troponin binding to Ca^{2+} is highest when the calcium concentration in the cytosol is lowest.

The shortening factor refers back to the concentration of $b_3^{(c)}(\boldsymbol{x}, t)$, the actin-myosin cross-bridges, and to the force that their linkage generates. It is scaled by the maximum possible contractile force $F_{\max}$, the actin stiffness k_s, and the proportion of active to inactive actin-myosin cross-bridges. As the proportion of active actin-myosin cross-bridges increases due to an increase in bounded troponin, the value of $b_{3,\text{total}}^{(c)} - b_3^{(c)} - [XB]_0$ increases. This results in a larger value of ε. As ε becomes larger, the rate at which the bounded troponin unbinds slows down. As described earlier, the lack of calcium provided by CRU resting periods results in a reset in this mechanism.

The contractile proteins in question, though considered as a single species, are the combination of actin and myosin when linked via cross-bridges. This linkage is made possible by Ca^{2+} binding to troponin, the cytosol buffer species $b_2^{(c)}(\boldsymbol{x}, t)$: it is this binding that allows the actin-myosin cross-bridges to form. The cytosol species, $b_3^{(c)}(\boldsymbol{x}, t)$, describes these actin-myosin cross-bridges and constructs a third cytosol reaction term

$$R_{b_3}^{(c)}(c, b_2^{(c)}, b_3^{(c)}) = -k_{b_3^{(c)}}^{+}\left(\frac{b_{2,\text{total}}^{(c)} - b_2^{(c)}}{b_{2,\text{total}}^{(c)}}\right)^2 b_3^{(c)} + k_{b_3^{(c)}}^{-}(b_{3,\text{total}}^{(c)} - b_3^{(c)}). \tag{12}$$

Notice that this is not the same as the generic pattern for buffer species reaction terms from the initial model. There is no immediately clear dependence on cytosolic calcium $c(\boldsymbol{x}, t)$. However, while $c(\boldsymbol{x}, t)$ is not explicitly included, it is present in the proportion involving troponin, $b_2^{(c)}(\boldsymbol{x}, t)$, which itself depends explicitly on cytosol calcium levels; $R_{b_3}^{(c)}$, like the other two reaction equations, does in fact depend on the cytosol calcium concentration. Unlike the other two reaction equations, $R_{b_3}^{(c)}$ indirectly impacts calcium levels.

These two reaction terms (10) and (12) connect the three components of our model. The calcium signaling is linked to the pseudomechanical contraction by the cross-bridge term, and the pseudo-mechanical contraction is in turn connected to the calcium signaling through the inclusion of the cytosol calcium concentration in the modified reaction equation for troponin. Thus links ①–④ in Figure 1 are established, and the three systems of the model are fully linked.

Note that in the reaction terms (9), (10), and (12), $b_1^{(c)}$, $b_2^{(c)}$, and $b_3^{(c)}$ are the amounts of *unbound* buffer known as "free" buffer. The constants $b_{i,\text{total}}^{(c)}$, $i = 1, 2, 3$, denote the *total bound and unbound* buffer, thus leaving the differences $b_{i,\text{total}}^{(c)} - b_i{}^{(c)}$ in the reaction terms to be the buffer *bound* with cytosol calcium c. Since the model uses no-flux boundary conditions, no buffer species escapes or enters the cell; thus we only need to track the "free" buffer species and use $b_{i,\text{total}}^{(c)} - b_i{}^{(c)}$ for the bound species. The values for the constants $b_{i,\text{total}}^{(c)}$, $i = 1, 2, 3$, are model parameters and specified in Table 2.

The flux terms J_{CRU}, J_{leak}, and J_{pump} in (1) describe the calcium-induced release of Ca^{2+} into the cytosol from the SR, the continuous leak of Ca^{2+} into the cytosol from the SR, and the pumping of Ca^{2+} back into the SR from the cytosol. The terms J_{LCC}, $J_{m_{\text{leak}}}$, and $J_{m_{\text{pump}}}$ describe the fluxes of calcium into and out of the cell via the plasma membrane. The coupling between (1) and (5) is achieved by the three flux terms shared by both.

More precisely, J_{LCC}, $J_{m_{\text{leak}}}$, and $J_{m_{\text{pump}}}$ in (1) describe the fluxes of calcium into and out of the cell via the plasma membrane. J_{pump} replenishes the calcium stores in the SR; it increases SR calcium concentration by decreasing cytosol calcium concentration. J_{leak} is a continuous leakage of those SR calcium stores into the cytosol; it increases cytosol concentration by decreasing SR calcium concentration. The pump term

$$J_{\text{pump}}(c) = V_{\text{pump}}\left(\frac{c^{n_{\text{pump}}}}{K_{\text{pump}}^{n_{\text{pump}}} + c^{n_{\text{pump}}}}\right) \tag{13}$$

is thus a function of cytosol calcium $c(\boldsymbol{x}, t)$. The leak term J_{leak} is a constant defined by

$$J_{\text{leak}} = J_{\text{pump}}(c_0), \tag{14}$$

which balances $J_{\text{pump}}(c)$ at basal level $c_0 = 0.1\ \mu\text{M}$ of cytosol calcium. The pump term J_{pump}, a function of cytosolic calcium $c(\boldsymbol{x}, t)$, consists of the maximum pump

velocity V_{pump} multiplied against the relationship between $c(\boldsymbol{x}, t)$ and the pump sensitivity K_{pump}; the exponent n_{pump} refers to the Hill coefficient (quantifying the degree of cooperative binding) for the pump function. This has the practical effect of multiplying the maximum possible pump velocity against a number between 0 and 1, exclusive. J_{leak}, which continuously leaks calcium into the cytosol from the SR, is simply J_{pump} evaluated at the basal cytosolic calcium concentration $c_0 = 0.1\ \mu\text{M}$. As noted, J_{pump} has two roles, namely to balance J_{leak} in the absence of sparking, but also to balance J_{CRU} under conditions of active calcium release.

The term J_{CRU} in (1) is the Ca^{2+} flux into the cytosol from the SR via each individual point source at which a CRU has been assigned. The effect of all CRUs is modeled as a superposition such that

$$J_{\text{CRU}}(c, s, \boldsymbol{x}, t) = \sum_{\hat{\boldsymbol{x}} \in \Omega_s} \hat{\sigma} \frac{s(\boldsymbol{x}, t)}{s_0} \mathcal{O}(c, s) \delta(\boldsymbol{x} - \hat{\boldsymbol{x}}), \tag{15}$$

with

$$\mathcal{O}(c, s) = \begin{cases} 1 & \text{if } u_{\text{rand}} \leq J_{\text{prob}}, \\ 0 & \text{if } u_{\text{rand}} > J_{\text{prob}}, \end{cases} \tag{16}$$

where

$$J_{\text{prob}}(c, s) = P_{\max} \left(\frac{c^{n_{\text{prob}_c}}}{K_{\text{prob}_c}^{n_{\text{prob}_c}} + c^{n_{\text{prob}_c}}} \right) \left(\frac{s^{n_{\text{prob}_s}}}{K_{\text{prob}_s}^{n_{\text{prob}_s}} + s^{n_{\text{prob}_s}}} \right). \tag{17}$$

The effect of each CRU is modeled here as a product of three terms:

(i) Similarly to how in J_{pump} the maximum pump rate is scaled against the concentration of available cytosol calcium, the maximum pump rate is scaled against the concentration of available cytosol calcium and the maximum rate of Ca^{2+} release $\hat{\sigma}$ is scaled here against the ratio of calcium concentration in the SR.

(ii) Following the same pattern, a maximum value multiplied against some scaling proportion between 0 and 1, the gating function $\mathcal{O}(c, s)$ has the practical effect of "budgeting" the calcium SR stores such that when the stores are low, the given CRU becomes much less likely to open; each CRU is assigned a uniformly distributed random value u_{rand}, which is compared to the single value returned by the CRU opening probability J_{prob} to determine whether or not the given CRU will open. J_{prob} is characterized by traits of CRUs CRU, which open for 5 ms and then proceed to close and remain in a refractory state for the following 100 ms.

(iii) The Dirac delta distribution $\delta(\boldsymbol{x} - \hat{\boldsymbol{x}})$ models each CRU as a point source for calcium release, which is defined by requiring $\delta(\boldsymbol{x} - \hat{\boldsymbol{x}}) = 0$ for all $\boldsymbol{x} \neq \hat{\boldsymbol{x}}$ and $\int_{\mathbb{R}^3} \psi(\boldsymbol{x}) \delta(\boldsymbol{x} - \hat{\boldsymbol{x}})\, d\boldsymbol{x} = \psi(\hat{\boldsymbol{x}})$ for any continuous function $\psi(\boldsymbol{x})$.

The linking between calcium signaling and electrical excitation consists of (6)–(7). The membrane potential of the cell depends on both the cytosol calcium ion concentration and also on the cytosol potassium ion (K^+) concentration [Banyasz

et al. 2012; Morris and Lecar 1981]. In our model, the ω-term in (6) quantifies a dependence of V on c to complete the coupling from the chemical to the electrical systems in link ② in Figure 1 [Angeloff et al. 2016], after c in (1) already contains several terms that depend on V to implement link ① in Figure 1. The Ca^{2+} conductance is much faster than the K^+ conductance, so the calcium conductance can be approximated as m_∞ or instantaneously steady-state at all times; the potassium conductance requires a separate description in (7). Needed parameter functions in (6)–(7) are

$$m_\infty(V) = \frac{1}{2}\left(1 + \tanh\left(\frac{V - V_1}{V_2}\right)\right), \tag{18}$$

$$n_\infty(V) = \frac{1}{2}\left(1 + \tanh\left(\frac{V - V_3}{V_4}\right)\right). \tag{19}$$

The connection between (1) and (6), link ① in Figure 1, the link from the electrical system to the calcium system, comes through

$$J_{\mathrm{LCC}} = \frac{\tau_{\mathrm{flux}}}{2F} S g_{\mathrm{Ca}} m_\infty(V)(V - V_{\mathrm{Ca}}), \tag{20}$$

the only calcium flux term to involve voltage. Note the parameter κ in (1), which is an external scaling factor for J_{LCC} rather than an intrinsic physiological component; if the value of κ is set to 0, the connection, link ① in Figure 1, is effectively switched off and the calcium dynamics are then modeled as though voltage were not involved. The surface area, S, of the cell is included in light of the fact that J_{LCC} describes the influx of calcium through L-type calcium channels (LCCs), which are present in the enclosing plasma membrane of the cell: the surface area of the cell is the surface area of the membrane.

We model the effect of the cytosol calcium concentration on the voltage by treating the calcium efflux term $J_{m_{\mathrm{pump}}} - J_{m_{\mathrm{leak}}}$ as equivalent to the sodium-calcium exchanger current: we are thus able to describe the current generated by the sodium-calcium exchange as a function of simple calcium loss.

The individual components of the calcium efflux term are near-duplicates in form of the earlier J_{pump} and J_{leak} functions in (13) and (14), respectively. As J_{pump} described the removal of calcium from the cytosol and its transfer into SR stores,

$$J_{m_{\mathrm{pump}}}(c) = V_{m_{\mathrm{pump}}}\left(\frac{c^{n_{m_{\mathrm{pump}}}}}{K_{m_{\mathrm{pump}}}^{n_{m_{\mathrm{pump}}}} + c^{n_{m_{\mathrm{pump}}}}}\right) \tag{21}$$

describes the removal of calcium from the cytosol and its transfer to outside the cell across the membrane. The leak term J_{leak} described a gradual leak of calcium into the cytosol from the SR, while J_{CRU} described an abrupt, high-concentration (high relative to the leak) release of calcium into the cytosol from the SR. Similarly,

$$J_{m_{\mathrm{leak}}} = J_{m_{\mathrm{pump}}}(c_0) \tag{22}$$

describes a gradual leak of calcium into the cytosol from outside the cell via the plasma membrane, while J_{LCC} describes a sudden spike of calcium release into the cytosol via the LCCs.

The seven-variable model presented in this section reduces to the three-variable model in the original sources [Izu et al. 2001a; 2001b] by the following choices: setting $\gamma = 0$, $\tau_v = 0$, $\omega = 0$, $\kappa = 0$, and $F_{\max} = 0$. With these parameters set to 0, links ①, ②, ③, and ④ in Figure 1 are all cut off.

3. Numerical method

In order to do calculations for the CICR model, we need to solve a system of time-dependent parabolic partial differential equations (PDEs). These PDEs are coupled by several nonlinear reaction and source terms. The current simulations use $n_s = 7$ physiological variables in (1)–(7). The domain in our model is a hexahedron Ω in (8) with isotropic CRU distribution as shown in Figure 2. A typical cell has on the order of $15 \times 15 \times 31 = 6{,}975$ calcium release units (CRUs) throughout the cell. A cell is reasonably modeled by the hexahedral shape elongated in the z-direction, since the focus of CICR research is on estimating correct physiological parameter values. Taking a method of lines (MOL) approach [Strikwerda 2004] to spatially discretize this model, we use the finite volume method (FVM) as the spatial discretization to ensure mass conservation on the discrete level and also to accommodate advection terms in the future, with $N = (N_x + 1)(N_y + 1)(N_z + 1)$ control volumes. Applying this to the case of the n_s PDEs results in a large system of ordinary differential equations (ODEs). A MOL discretization of a diffusion-reaction equations with second-order spatial derivatives results in a stiff ODE system. The time step size restrictions, due to the CFL condition, are considered too severe to allow for explicit time-stepping methods. This necessitates the use of a sophisticated ODE solver such as the family of implicit numerical differentiation formulas (NDFk). We use Newton's method as the nonlinear solver, and at each Newton step we use the biconjugate gradient stabilized method (BiCGSTAB) or other Krylov subspace methods as the linear solver. Complete details of the numerical method can be found in [Schäfer et al. 2015].

While the form of the PDEs in (1)–(7) is customary, the thousands of point sources at the calcium release units (CRUs) in the forcing terms imply that standard codes have difficulty. This explains why our research centered around creating a special-purpose code [Gobbert 2008; Hanhart et al. 2004; Seidman et al. 2012; Schäfer et al. 2015]. Additionally, we leverage the regular three-dimensional shape of the domain to program all methods in matrix-free form. Table 4 demonstrates thus, how despite fully implicit time-stepping, even relatively fine meshes use only reasonable amounts of memory. This provides the key benefit now for the complete

mesh resolution $N_x \times N_y \times N_z$	N	DOF n_{eq}	time steps	memory (GB) predicted	memory (GB) observed
$32\times32\times128$	140,481	983,367	2667	0.125	< 1
$64\times64\times256$	1,085,825	7,600,775	3295	0.963	1.093
$128\times128\times512$	8,536,833	59,757,831	3867	7.569	8.476
$256\times256\times1024$	67,700,225	473,901,575	4470	60.024	67.103

Table 4. Sizing study with $n_s = 7$ variables using double precision arithmetic, listing the mesh resolution $N_x \times N_y \times N_z$, the number of control volumes $N = (N_x+1)(N_y+1)(N_z+1)$, the number of degrees of freedom (DOF) $n_{\text{eq}} = n_s N$, the number of time steps taken by the ODE solver up to final time $t_{\text{fin}} = 100\,\text{ms}$, and the predicted and observed memory usage in GB for a one-process run.

complex model with complete sophisticated numerical method stack, even with 7 or 8 variables, to fit into the memory of a single cluster node with extended memory. The table also shows how large the number of degrees of freedom (DOF) is, that is, the number of variables that have to be computed at every time step. With even modest meshes, there are millions of unknowns, and possibly hundreds of millions for fine meshes. This characterizes the numerical problem that needs to be tackled to resolve the large number of thousands of calcium release units (CRUs) in a cell. Note that Table 4 presents a numerical test on a shortened time frame with final time $t_{\text{fin}} = 100\,\text{ms}$, which is large enough to include significant nonlinear behavior, but small enough to allow for reasonable run times. In the following result sections, final times of $t_{\text{fin}} = 1{,}000\,\text{ms}$ and $t_{\text{fin}} = 5{,}000\,\text{ms}$ are used, as specified in the subsections as well as summarized in Table 5

The implementation of this model is done in C using MPI and OpenMP to parallelize computations. Parallelization is accomplished through the block-distribution of all large arrays to all MPI processes. We split of the mesh in the z-direction with one subdomain on each of the parallel processes. MPI commands such as `MPI_Isend` and `MPI_Irecv`, which are nonblocking point-to-point communication commands, send messages between neighboring processes. The collective command `MPI_Allreduce` is used for the computation of scalar products and norms.

4. Results

This section shows the results of simulations for the seven-variable model detailed in Section 2 with variables and their values at the initial time $t = 0\,\text{ms}$ specified in Table 1. The following subsections show physiological output that is possible through long-time computational simulations to a final time that is large enough

parameter	base case Sec. 4.1	SR store Sec. 4.2	voltage system Sec. 4.3	mechanical system Sec. 4.4	Sec. 4.5
γ	0.0	0.01 to 1000	14.0	14.0	14.0
τ_v	0.0	0.0	0.1	0.1	0.1
$V_{m_{\text{pump}}}$	0.0	0.0	0.001 to 1	0.3	0.3
ω	0.0	0.0	0.1 to 1000	100.0	100.0
κ	0.0	0.0	0.001 to 10	0.1	0.1
$F_{\max}$	0.0	0.0	0.0	0.001 to 100	1,100
t_{fin}	1000	1000	1000	1000	5000

Table 5. Parameter differences between cases in this section.

to include several calcium waves. Tables 2 and 3 specify all model parameters, their names, and their values or ranges with units, except certain parameters that are varied in this section. Table 5 specifies for each of the subsections, what values are used. In Tables 2 and 3, the values of the variables are selected from Table 5. Section 4.1 connects to the original modeling in [Izu et al. 2001a; 2001b] by performing simulations with parameters chosen such that the seven-variable model reduces to the original three-variable model used in these papers. Sections 4.2, 4.3, and 4.4 successively vary parameters shown in Table 5, in addition to the parameter changes made in the previous subsections. This approach allows for the construction of the entire model by adding new components on top of previous ones. With the entire model pieced together, we can test the model as a whole. Section 4.5 briefly exhibits the power of the physiologically connected model by showing the impact of $F_{\max} = 1$ and $F_{\max} = 100$ on the entire system for $t = 5{,}000$ ms, a longer duration of time. These results show the power of the model with the physiologically linked components and motivate further studies using this model.

4.1. ***Base case.*** The seven-variable model in (1)–(7) reduces to the three-variable model in the original sources [Izu et al. 2001a; 2001b] by the following choices: setting $\kappa = 0$, $F_{\max} = 0$, and $\gamma = 0$. When looking at the seven equations, changing these parameters to zero is most appropriate as they result in removing the calcium store in the sarcoplasmic reticulum (SR) and the effects of mechanical contraction.

The final addition of the three-variable model, electrical excitation, can be absolutely removed by setting (6) and (7) to zero. Changing $\tau_v = 0$ achieves this. These three components are only unique to the seven-variable model. To confirm that the first equation, (1), acts identically to the first equation in [Izu et al. 2001a], we must be absolutely sure that $J_{m_{\text{leak}}} - J_{m_{\text{pump}}} = 0$. To do this, we change $V_{m_{\text{pump}}} = 0$ and $\omega = 0$, resulting in (21) negating to zero and both sides of (22) equaling zero.

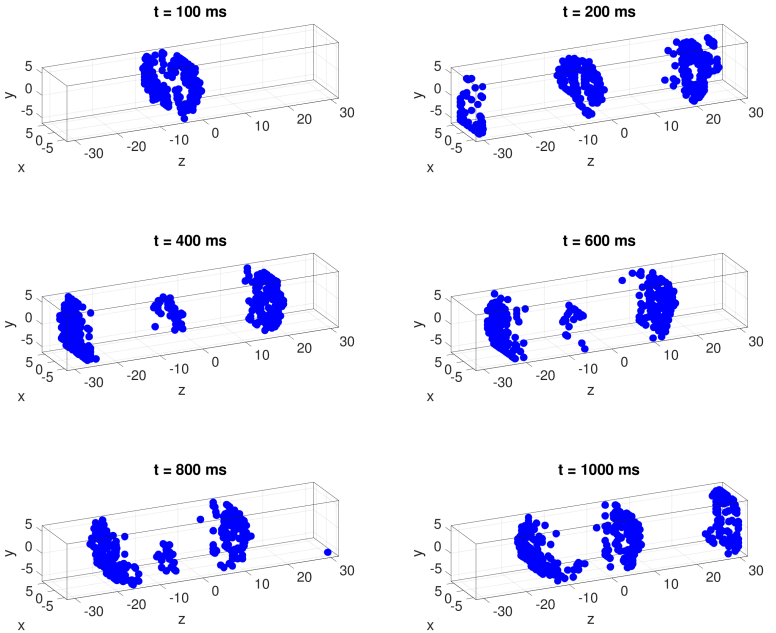

Figure 3. Open calcium release units throughout the cell.

With these additional changes, the seven-variable model functions identically to the three-variable model in the original sources [Izu et al. 2001a; 2001b].

The first set of plots, in Figure 3, display the locations of open calcium release units by a dot. The more dark dots are visible, the more CRUs are open at that specific time. More specifically, since one open CRU tends to promote neighboring CRUs to open through the diffusion of calcium, a clustering of dots indicates a region of several open CRUs. Note that we start with initial conditions in Table 5 for which there are no open CRUs and the right-hand sides of all equations in (1)–(7) are zero. Thus, these simulations represent a study in spontaneous sparking, in which some CRUs happen to open according to the probabilistic model in (15)–(17). This model embodies the effect of a higher concentration of cytosol calcium increasing the probability for a CRU to open in (17). The result of this spontaneous self-initiation is seen in the first subplot in Figure 3, where a number of CRUs in one region of the cell have opened by $t = 100$ ms. The study of self-initiation was the original purpose of this model of calcium-induced calcium releases [Izu et al. 2001a; 2001b] and only required modest final times. The extension of the simulations to larger final times allows us to study if the opening and closing of CRUs self-organizes into a sustained wave. This is seen in the following subplots in Figure 3. The model requires CRUs to close for 100 ms after opening for 5 ms; thus the subplots indicate that the original cluster of open CRUs travels in both

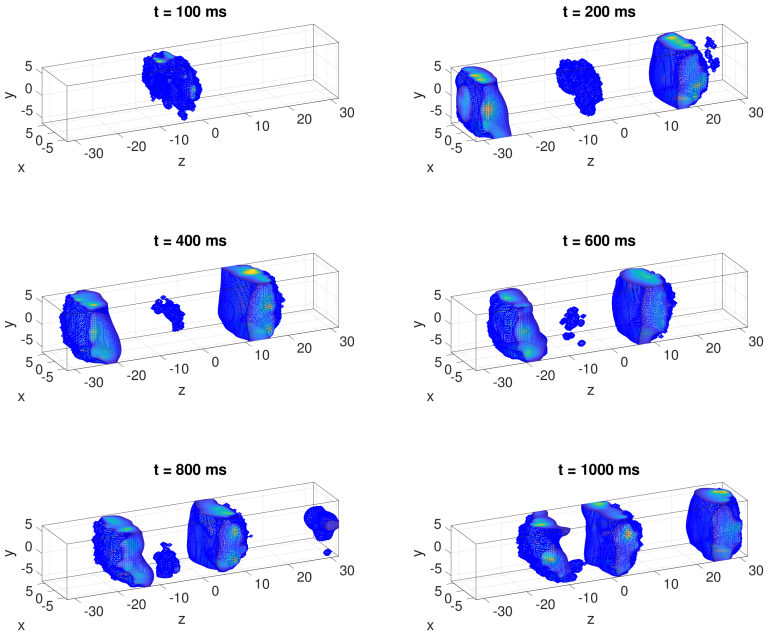

Figure 4. Concentration of $c(\boldsymbol{x}, t)$ with a critical value of 65 μM.

directions through the elongated direction of the cell and roughly repeats every 100 ms. Movies of the full results including intervening times confirm this behavior.

Figure 4 shows a collection of isosurface plots for calcium concentration in the cytosol. An isosurface plot displays the surface in the three-dimensional cell, where the species concentration is equal to a critical value, stated in the caption of the figure, here 65 μM for the concentration of cytosol calcium $c(\boldsymbol{x}, t)$. Blue represents when the species' concentration equals 65 μM. For densities lower than 65 μM, there are no markings. More extreme concentrations of each species are indicated with the spectrum from yellow to red, where darker hues are more intense in density. As we can see from the subplots in Figure 3, we have an original cluster in the middle at $t = 100$ ms that diffuses towards the ends of the cell and repeats on a 100 ms cycle. Due to the connection of the calcium in the cytosol with open CRUs through the effect of calcium-induced calcium release, calcium concentrations in the cytosol corresponds to locations of open CRUs.

This physiological concept is shown with each subplot in Figure 4, where the species' concentration colors are in agreement with the amount of open CRUs in Figure 3 at that time.

The concentrations of $b_1^{(c)}(\boldsymbol{x}, t)$ and $b_2^{(c)}(\boldsymbol{x}, t)$ have the same characteristics as the calcium levels in the cytosol since they are all influenced in the same way; therefore, we do not show them. The remaining isosurface plots for the base case are not

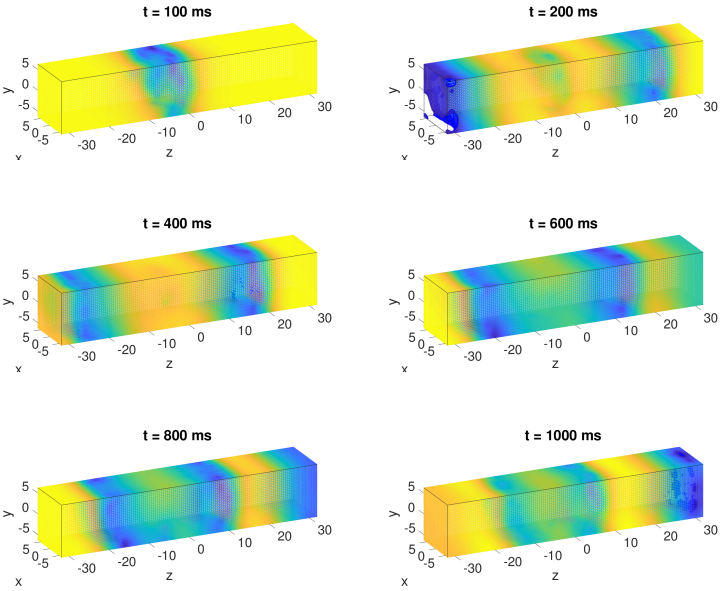

Figure 5. Concentration of $s(\boldsymbol{x}, t)$ with a critical value of 5000 μM.

included because each of the additional species' concentrations remain constant. Thus each subplot remains uneventful. As the CICR components are added to the base case in the following subsections, the respective isosurface plots will also be included.

4.2. ***Adding the calcium store in the sarcoplasmic reticulum (SR).*** To add the calcium store in the sarcoplasmic reticulum (SR), (5) must provide nonconstant concentrations of calcium. We can set $\gamma = 14$ to remove the previous reduction of this equation in Section 4.1. These values for γ and D_s are from Table 5.

We can look at the isosurface plots for calcium in the SR to determine the functionality of the calcium store in the SR with the two changed parameters. The seven equations allow for a range of concentrations for calcium in the SR from 0.01 to 10,000 μM. Figure 5 shows a collection of isosurface plots for calcium concentration in the SR with a critical value of 5,000 μM. Concentrations more extreme than the critical value are represented with a spectrum start from blue to yellow, where yellow represents concentrations closest to the maximum. When looking at Figure 5 the lighter concentrations of calcium in the SR directly correspond to the extreme concentrations of calcium throughout the cell.

Figure 5 shows that the calcium store was implemented. Unlike in Section 4.1 where the concentration of calcium in the SR remained constant at 10,000 μM, the subplots in Figure 5 contain numerous examples of varying concentration of calcium in the SR.

The choice of $\gamma = 14$ was determined through an analysis of several other cases with different values for γ. From the range that was tested, 0.01 to 1000, every value eventually resulted in continuous calcium waves. This is expected as adding to the calcium store does not hinder the continuous calcium waves. However, γ-values of 100 and above resulted in a range of calcium concentration in the SR that included negative values. The seven-equation model is limited for large γ-values as it does not account for negative concentrations, which physiologically are inconceivable. Simulations for γ-values 1 and below resulted in insignificant changes to the calcium in the SR, showing that the smaller values of γ do not sufficiently add to the decrease in calcium from the store according to the increase of calcium in the cytosol. From the parameter study, $\gamma = 10$ was idealistic, as continuous calcium waves are apparent and an appropriate calcium store was successfully implemented. In this paper, $\gamma = 14$ is used to keep consistency with previous studies that used $\gamma = 10$. No significant differences can be found between $\gamma = 14$ and $\gamma = 10$.

The CRU plots and the isosurface plots for $c(\boldsymbol{x}, t)$, $b_1^{(c)}(\boldsymbol{x}, t)$, and $b_2^{(c)}(\boldsymbol{x}, t)$ remained nearly identical to the plots in Section 4.1 This shows that the implementation of the calcium store did not heavily influence the concentrations of free fluorescent dye from (2) and free troponin from (3).

4.3. ***Adding the effect of electrical excitation.*** Implementing the effect of electrical excitation on top of the calcium store in the SR is achieved through activating (6) and (7). From the reduced version of the seven-variable model, setting $\tau_v = 0.1\,\mu\text{M}\,\mu\text{m}^3/\text{ms}$, $V_{m_{\text{pump}}} = 0.3\,\mu\text{M/ms}$, $\omega = 100$, and $\kappa = 0.1$ results in functional equations for electrical excitation. We can make several other cases with various values of each varied parameter to see how different extremes for each variable changes the resulting calcium wave.

From Section 4.2, we performed three separate one-dimensional studies in order to find values for $V_{m_{\text{pump}}}$, ω, and κ that fully add the voltage system without significant changes to the various species' concentrations in Section 4.2.

The first one-dimensional study varied $V_{m_{\text{pump}}}$ from 0.001 to 1. Changing this parameter to a fixed value allows for the functionality of the function (21) and consequently (22). Both $V_{m_{\text{pump}}}$ and $V_{m_{\text{leak}}}$ have an influence on (1) and (6). From this study, the largest value that retains the continuous calcium waves described in Section 4.1 was $V_{m_{\text{pump}}} = 0.3\,\mu\text{M/ms}$.

With this fixed value for $V_{m_{\text{pump}}}$, we can perform a one-dimensional study of ω, the feedback strength for Ca^{2+} efflux, and an additional study of κ. When varying ω, we noted that from $\omega = 0.1$ to 1000, the CRU plots are almost identical to our CRU plots from Section 4.2. As such, we can set $\omega = 100.0$, a fixed value, as all tested cases of ω simulated similar results to the plots shown in Section 4.2.

To fully implement the voltage system, we need to test values of κ to find what nonzero value of κ would allow for continuous calcium waves with a fully

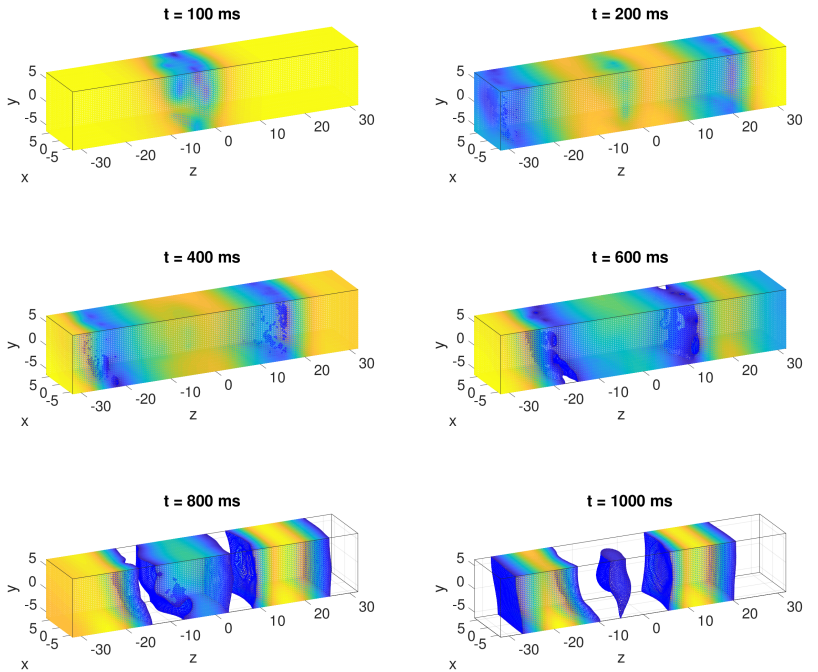

Figure 6. Concentration of $s(\boldsymbol{x}, t)$ with a critical value of 5000 μM.

implemented voltage system and calcium in the SR. When varying κ from 0.001 to 10, we noted that $\kappa = 0.1$ was the largest value in which the calcium waves were comparable to the previous subsections.

Setting $\kappa = 0.1$, $\omega = 100$, $\tau_v = 0.1\ \mu\text{M}\,\mu\text{m}^3/\text{ms}$, and $V_{m_{\text{pump}}} = 0.3\ \mu\text{M/ms}$ in addition to the predetermined values for the parameters in Table 5 allows for the full implementation of the voltage system without fundamentally changing the outflow of calcium.

The CRU plots and the isosurface plots for $c(\boldsymbol{x}, t)$, $b_1^{(c)}(\boldsymbol{x}, t)$, and $b_2^{(c)}(\boldsymbol{x}, t)$ did not significantly change with the implementation of the voltage system. However, there are more notable differences when comparing the calcium concentrations of the stores shown in Figures 6 and 5. In Figure 6, the latter plots have colorless space between each clump of calcium. As these spaces are representative of lower calcium concentrations, these plots show that the store in the SR has lower concentrations of calcium. Larger time studies may indicate that the calcium concentration in the store continues to lower past $t = 100$ ms.

The voltage plot in Figure 7 shows that the electrical system was implemented. The voltage plots from the previous subsections remained constant at -50 mV. In Figure 7, there is a clear repetition of the voltage rising up to approximately 26 mV back down to approximately -23 mV. This figure confirms that external voltage is

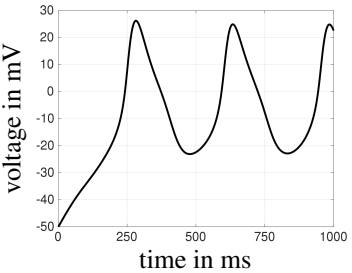

Figure 7. Voltage levels throughout the cell over period of 1000 ms.

present. Based on these comparisons, these plots maintain the same behaviors from Section 4.2 with the addition of the voltage system.

4.4. ***Adding the effect of mechanical contraction.*** In the seven-variable model, mechanical contraction is described through (3) and (4). From the parameters added in Section 4.3 shown in Table 5, a parameter study was performed on the values for $F_{\max}$. By changing this parameter to nonzero values, we can study the effects of mechanical contraction on top of the previously included calcium store and electrical excitation. In addition to these set values, we created other cases with various values for $F_{\max}$ to note the physiological changes with various values of (3) and (4).

For this parameter study, we tested a range from $F_{\max} = 0.001$ to $F_{\max} = 100$. For $F_{\max}$ values less than 1, the shortening factor remained the same, where after about 125 ms ε began to cycle between a small range and remained this way up to 1000 ms. For $F_{\max} = 100$, the shortening factor loses its period; that is, the value does not cycle. Rather, the shortening factor spikes up two times throughout the 1,000 ms. While $F_{\max} = 10$ maintains the cycling value of the shortening factor, there is an apparent delay for the cycle to begin. Unlike the start time of 125 ms for the lower values of $F_{\max}$, for $F_{\max} = 10$, the start time is 250 ms. Since the simulations are only 1,000 ms in length, the desired value for $F_{\max}$ is 1.

As in the previous subsections, the CRU plots and the isosurface plots for $c(\boldsymbol{x}, t)$, $b_1^{(c)}(\boldsymbol{x}, t)$, and $b_2^{(c)}(\boldsymbol{x}, t)$ appear to be extremely similar if not identical to plots from the previous subsections. Additionally, the concentrations shown in Figures 6 and 7 remain the same with the addition of $F_{\max}$. This shows that the implementation of the mechanical contraction did not heavily influence the other components to the extent of changing the system.

With $F_{\max}$ set to a nonzero value, the shortening factor, described in (11), is able to vary based on inactive actin-myosin cross-bridges described in (4). In the previous subsections, the lack of the variance in the shortening factor led to the inability of the continuous contractions of the cross-bridges to take place. Unlike the previous subsections, this shortening factor is able to vary in severity, allowing for the repetition of inactive cross-bridges switching to active ones. This repetitive cycle

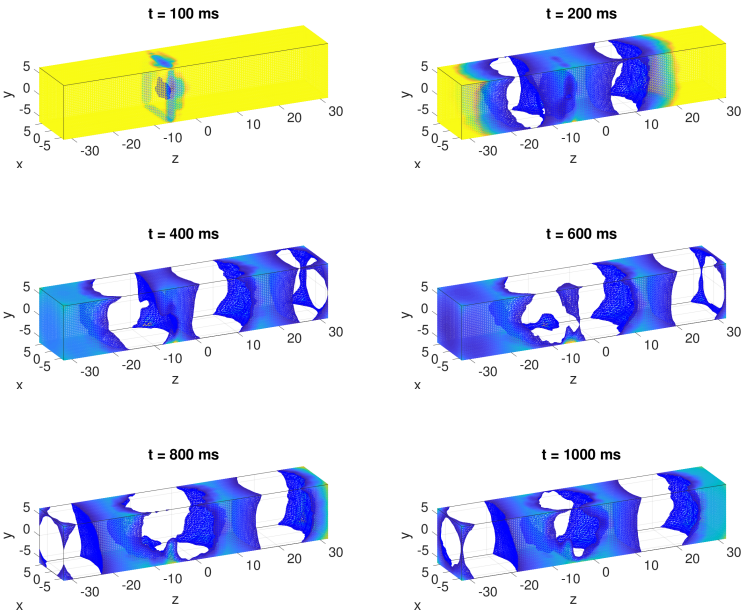

Figure 8. Concentration of $b_3^{(c)}(\boldsymbol{x}, t)$ with a critical value of 50 μM.

is displayed in Figure 8. In previous subsections, the plots for inactive actin-myosin cross-bridges remained constant throughout the 1,000 ms.

As in the previous subsections, the CRU plots and the isosurface plots for $c(\boldsymbol{x}, t)$, $b_1^{(c)}(\boldsymbol{x}, t)$, and $b_2^{(c)}(\boldsymbol{x}, t)$ appear to be extremely similar to plots from the previous subsections. Additionally, the concentrations shown in Figures 6 and 7 remain the same with the addition of $F_{\max}$ This shows that the implementation of the mechanical contraction with the so-far chosen parameters did not heavily influence the other components to the extent of changing the system.

4.5. ***Influence of $F_{\max}$ on the entire system.*** With these set parameters described in Section 4.1, we are able to test questions retaining to the entire model. One example of this is the study of $F_{\max}$ for the much longer final time $t_{\text{fin}} = 5{,}000$ ms rather than 1,000 ms on the seven-variable model. From the tested values for $F_{\max}$ from 0.001 to 100, values 1 and 100 are shown in the plots below. These values were determined through the parameter study of $F_{\max}$ from Section 4.4.

Figures 9 and 13 show plots of both the voltage V and shortening factor ε vs. time for the model. While the content is different, the structure of the voltage plots is identical to the voltage plots described in Section 4.3. The plots of the shortening factor ε vs. time track the value of the shortening factor, ε, used in (3).

There are several differences between how each $F_{\max}$ value affects the system. Figures 9–12 are representative of the same simulations as in Section 4.4, except the

duration of time was extended from $t_{\text{fin}} = 1{,}000$ ms to 5,000 ms. As previously described, around 125 ms the calcium concentration in the cytosol shown in Figure 10 jumps from 0 to slightly less than 4×10^5 and slowly decreases as the calcium concentration in the store depletes. In Figure 12, the calcium concentration in the store drops at the same time. The calcium concentration in the store continues to drop until about 2,500 ms, where it then levels out. The concentration of $b_3^{(c)}(\boldsymbol{x}, t)$ in Figure 11 drops at the same time as the calcium change in the cytosol. Once the calcium in the cytosol depletes, the concentration of $b_3^{(c)}(\boldsymbol{x}, t)$ returns to its initial state.

When comparing Figures 9–12 using $F_{\max} = 1$ and Figures 13–16 using $F_{\max} = 100$, there are clear differences. In Figure 14, the calcium concentration jumps from its initial state similarly to the calcium concentration of Figure 10. However, it shortly returns to its initial state and remains so for several hundred milliseconds before jumping back up. This spike back downward is not characterized in Figures 9–12. The concentration around 1,000 ms jumps up to nearly 9×10^5, more than double the peak concentration of calcium in the cytosol for $F_{\max} = 1$. Furthermore, the range of concentration levels in 100 ms is much larger than in Figure 10. The calcium in the store, shown in Figure 12, overall has a downward trend until around 3,000 ms, where the calcium concentration in the store levels out. The calcium concentration in the cytosol in Figure 10 correspondingly drops down to nearly 0. Similar to the first spike of calcium in Figure 10, in Figure 11, the concentration of $b_3^{(c)}(\boldsymbol{x}, t)$ drops with the spike and almost returns to its initial state before dropping a second time around 1,000 ms. The concentration remains relatively constant until the calcium in the cytosol drops. At this point the concentration of $b_3^{(c)}(\boldsymbol{x}, t)$ rises back up to the same concentration as its initial state and remains around that level until the final time $t_{\text{fin}} = 5{,}000$ ms.

There are also notable differences between the plots of the shortening factor ε vs. time in Figures 9 and 13. Both plots generally have the same characteristics as the plots of $b_3^{(c)}$. Where the value for ε is greater, the concentration of $b_3^{(c)}$ is lower. Between the plots in Figures 9 and 13, the range of oscillation is much smaller in Figure 13 than in Figure 9 during the period where the value of ε oscillates.

Unlike the other plots, the plots of voltage V vs. time in Figures 9 and 13 retain consistency throughout the entire 5,000 ms. The voltage level in both plots oscillates from a negative value to a positive value. It appears that the range of one oscillation of voltage shrinks slightly as the calcium levels in the cytosol increase. Other than this, it appears that the change in $F_{\max}$ does not have such a drastic impact on the characteristics of voltage compared to the concentrations of each species of the cell. As such, it appears that the influence of the mechanical system is directed towards calcium signaling and therefore has an indirect influence on voltage. This might be expected as there are no direct links between the mechanical system and electrical excitation.

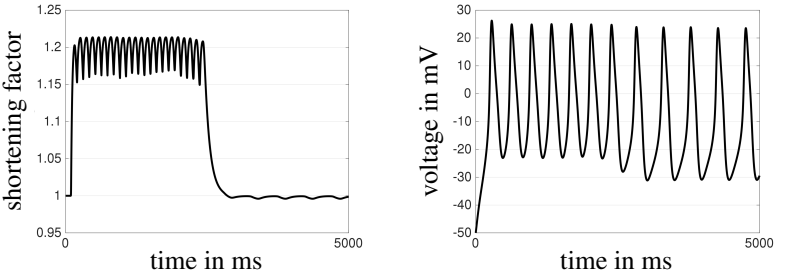

Figure 9. Plots of voltage V and shortening factor ε vs. time with $F_{\max} = 1$ for $t_{\text{fin}} = 5{,}000$ ms.

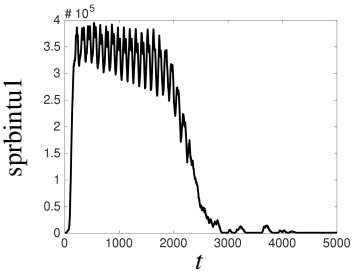

Figure 10. Total concentration of $c(\boldsymbol{x}, t)$ vs. time with $F_{\max} = 1$ for $t_{\text{fin}} = 5{,}000$ ms.

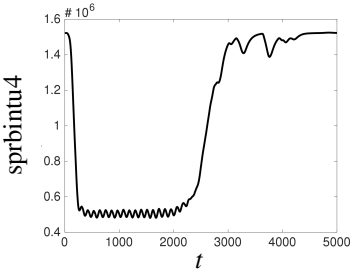

Figure 11. Total concentrations of $b_3^{(c)}(\boldsymbol{x}, t)$ vs. time with $F_{\max} = 1$ for $t_{\text{fin}} = 5{,}000$ ms.

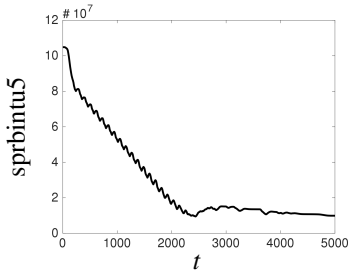

Figure 12. Total concentrations of $s(\boldsymbol{x}, t)$ vs. time with $F_{\max} = 1$ for $t_{\text{fin}} = 5{,}000$ ms.

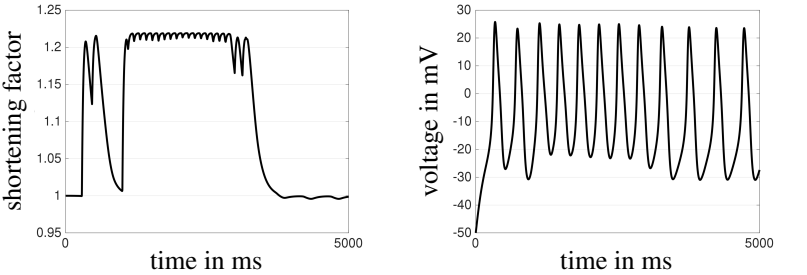

Figure 13. Plots of voltage V and shortening factor ε vs. time with $F_{\max} = 100$ for $t_{\text{fin}} = 5{,}000$ ms.

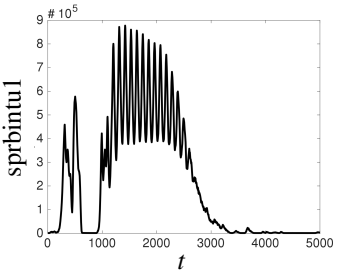

Figure 14. Total concentration of $c(\boldsymbol{x}, t)$ vs. time with $F_{\max} = 100$ for $t_{\text{fin}} = 5{,}000$ ms.

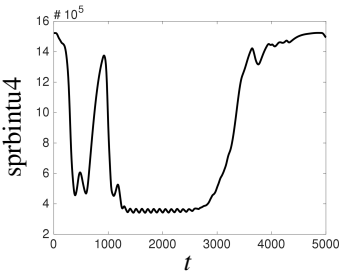

Figure 15. Total concentrations of $b_3^{(c)}(\boldsymbol{x}, t)$ vs. time with $F_{\max} = 100$ for $t_{\text{fin}} = 5{,}000$ ms.

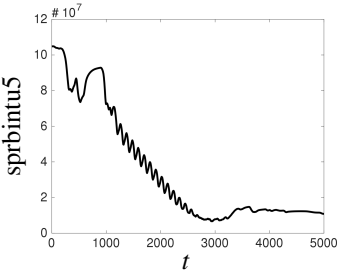

Figure 16. Total concentrations of $s(\boldsymbol{x}, t)$ vs. time with $F_{\max} = 100$ for $t_{\text{fin}} = 5{,}000$ ms.

5. Conclusions and outlook

We successfully created a table of parameters in Section 4 that allow for a more complete functioning model. This model includes the calcium store, electrical excitation, and mechanical contraction of the cardiac muscle cell. Unlike before, this table allows for the cohesion of all components of the model. With this, we are able to study the model in its entirety. As an example, we showed some influences of $F_{\max}$, a constant of the shortening factor, on the entire system over a period of 5,000 ms. When comparing small and large values for $F_{\max}$, we noticed that the influence of $F_{\max}$ was much less extreme on the electrical excitation compared to the calcium signaling. When comparing the plots of the relevant species of the system, this conclusion becomes apparent. This is important as it allows us to grasp a better understanding of the linkage between the mechanical system and calcium signaling, shown by link ① in Figure 1.

Future research on this could look more in depth at different values of other parameters with a final time of 5,000 ms. This would allow for studies on the system for longer periods of time. Studying multiple cases for each parameter value with randomized locations for calcium sparking would allow for more concrete conclusions with a stronger representation of the physiological processes of the cell. While this is one further area of study, this complete set of parameters opens many areas to study the model in its entirety.

Acknowledgements

The hardware in the UMBC High Performance Computing Facility (HPCF) is supported by the U.S. National Science Foundation through the MRI program (grant nos. CNS–0821258, CNS–1228778, and OAC–1726023) and the SCREMS program (grant no. DMS–0821311), with additional substantial support from the University of Maryland, Baltimore County (UMBC). See hpcf.umbc.edu for more information on HPCF and the projects using its resources. Barajas was supported by UMBC as HPCF RA.

References

[Alexander et al. 2015] A. M. Alexander, E. K. DeNardo, E. Frazier, III, M. McCauley, N. Rojina, Z. Coulibaly, B. E. Peercy, and L. T. Izu, "Spontaneous calcium release in cardiac myocytes: store overload and electrical dynamics", *Spora* **1**:1 (2015), 36–48.

[Angeloff et al. 2016] K. Angeloff, C. A. Barajas, A. Middleton, U. Osia, J. S. Graf, M. K. Gobbert, and Z. Coulibaly, "Examining the effect of introducing a link from electrical excitation to calcium dynamics in a cardiomyocyte", *Spora* **2**:1 (2016), 49–73.

[Banyasz et al. 2012] T. Banyasz, B. Horvath, Z. Jian, L. T. Izu, and Y. Chen-Izu, "Profile of L-type Ca^{2+} current and Na^{+}/Ca^{2+} exchange current during cardiac action potential in ventricular myocytes", *Heart Rhythm* **9**:1 (2012), 134–142.

[Deetz et al. 2017a] K. Deetz, N. Foster, D. Leftwich, C. Meyer, S. Patel, C. Barajas, M. K. Gobbert, and Z. Coulibaly, "Developing the coupling of the mechanical to the electrical and calcium systems in a heart cell", Technical Report HPCF–2017–15, High Performance Computing Facility, University of Maryland, Baltimore County, 2017, available at http://hdl.handle.net/11603/11308.

[Deetz et al. 2017b] K. Deetz, N. Foster, D. Leftwich, C. Meyer, S. Patel, C. Barajas, M. K. Gobbert, and Z. Coulibaly, "Examining the electrical excitation, calcium signaling, and mechanical contraction cycle in a heart cell", *Spora* **3**:1 (2017), 66–85.

[Gobbert 2008] M. K. Gobbert, "Long-time simulations on high resolution meshes to model calcium waves in a heart cell", *SIAM J. Sci. Comput.* **30**:6 (2008), 2922–2947. MR Zbl

[Hanhart et al. 2004] A. L. Hanhart, M. K. Gobbert, and L. T. Izu, "A memory-efficient finite element method for systems of reaction-diffusion equations with non-smooth forcing", *J. Comput. Appl. Math.* **169**:2 (2004), 431–458. MR Zbl

[Izu et al. 2001a] L. T. Izu, J. R. H. Mauban, C. W. Balke, and W. G. Wier, "Large currents generate cardiac Ca^{2+} sparks", *Biophysical J.* **80**:1 (2001), 88–102.

[Izu et al. 2001b] L. T. Izu, W. G. Wier, and C. W. Balke, "Evolution of cardiac calcium waves from stochastic calcium sparks", *Biophysical J.* **80**:1 (2001), 103–120.

[Morris and Lecar 1981] C. Morris and H. Lecar, "Voltage oscillations in the barnacle giant muscle fiber", *Biophysical J.* **35**:1 (1981), 193–213.

[Mozaffarian et al. 2015] D. Mozaffarian et al., "Heart disease and stroke statistics — 2015 update: A report from the american heart association", *Circulation* **131**:4 (2015), e29–e322.

[Schäfer et al. 2015] J. Schäfer, X. Huang, S. Kopecz, P. Birken, M. K. Gobbert, and A. Meister, "A memory-efficient finite volume method for advection-diffusion-reaction systems with nonsmooth sources", *Numer. Methods Partial Differential Equations* **31**:1 (2015), 143–167. MR Zbl

[Seidman et al. 2012] T. I. Seidman, M. K. Gobbert, D. W. Trott, and M. Kružík, "Finite element approximation for time-dependent diffusion with measure-valued source", *Numer. Math.* **122**:4 (2012), 709–723. MR Zbl

[Strikwerda 2004] J. C. Strikwerda, *Finite difference schemes and partial differential equations*, 2nd ed., Society for Industrial and Applied Mathematics, Philadelphia, PA, 2004. MR Zbl

Received: 2019-06-01 Revised: 2019-12-13 Accepted: 2020-01-06

gkroiz1@umbc.edu *Department of Mathematics and Statistics, University of Maryland, Baltimore County, Baltimore, MD, United States*

barajasc@umbc.edu *Department of Mathematics and Statistics, University of Maryland, Baltimore County, Baltimore, MD, United States*

gobbert@umbc.edu *Department of Mathematics and Statistics, University of Maryland, Baltimore County, Baltimore, MD, United States*

bpeercy@umbc.edu *Department of Mathematics and Statistics, University of Maryland, Baltimore County, Baltimore, MD, United States*

involve

msp.org/involve

INVOLVE YOUR STUDENTS IN RESEARCH

Involve showcases and encourages high-quality mathematical research involving students from all academic levels. The editorial board consists of mathematical scientists committed to nurturing student participation in research. Bridging the gap between the extremes of purely undergraduate research journals and mainstream research journals, *Involve* provides a venue to mathematicians wishing to encourage the creative involvement of students.

See inside back cover or msp.org/involve for submission instructions. The subscription price for 2020 is US $205/year for the electronic version, and $275/year (+$35, if shipping outside the US) for print and electronic. Subscriptions, requests for back issues and changes of subscriber address should be sent to MSP.

Involve (ISSN 1944-4184 electronic, 1944-4176 printed) at Mathematical Sciences Publishers, 798 Evans Hall #3840, c/o University of California, Berkeley, CA 94720-3840, is published continuously online. Periodical rate postage paid at Berkeley, CA 94704, and additional mailing offices.

Involve peer review and production are managed by EditFlow® from Mathematical Sciences Publishers.

PUBLISHED BY

mathematical sciences publishers

nonprofit scientific publishing

http://msp.org/

involve
2020 vol. 13 no. 3